ANALYSIS OF CURRENT-MODE CONTROLLED PWM CONVERTERS USING THE MODEL OF THE CURRENT-CONTROLLED PWM SWITCH

Vatché Vorpérian

Electrical Engineering Department
Virginia Tech
Blacksburg, Virginia 24061

ABSTRACT

The switching and control actions in current-mode controlled PWM converters are attributed to a three-terminal switching device called the current-controlled PWM switch (CC-PWM.) An equivalent circuit model of the CC-PWM switch is derived to determine the dc and small-signal characteristics of current-mode controlled dc-to-dc converters. This model, like the model of the PWM switch given earlier by the author, is self-contained, accurate and easy to use. An interesting feature of the model is the simplicity with which it explains the sub-harmonic oscillation in constant frequency current-programmed converters. The model shows that, regardless of the particular topology, the dynamics of the current loop is always given by a parallel resonant circuit centered at half the switching frequency whose damping, among other things, depends on the duty-ratio and the external ramp. In the absence of an external ramp, as the duty-ratio is increased beyond fifty-percent the damping becomes negative and the circuit oscillates at half the switching frequency.

INTRODUCTION

Pulse-Width-Modulated dc-to-dc converters provide regulated dc voltages by the application of a single feedback loop from the output voltage to the duty-ratio control circuit. The addition of a second feedback loop from the switch current, known as current mode control, provides several advantages over single-loop or voltage-mode control. Short circuit protection and parallel operation of several converters are among the obvious advantages. Current-mode control can also provide improved small-signal characteristics. Since their introduction [1], it has been known that constant frequency current-mode controlled converters break into sub-harmonic oscillations under certain operating conditions which can not be adequately explained by simple continuous-time models [2],[3] and [4]. Nevertheless, the nature of these oscillations were well understood using simple arguments and a remedy had been devised. Examining the relationship between the inductor current, its slopes and the control voltage it was seen that the addition of an external ramp to the natural ramp of the inductor current during the on-time would eliminate the unwanted sub-harmonic oscillations. An accurate explanation of the small-signal behavior of current mode control was given using sampled-data analysis [5]. The rather elaborate formulation of sampled-data analysis does not provide physical insight and is difficult to use towards design purposes. A simple, accurate and continuous-time model for current mode control was given recently [6,7] which predicts all the desired small-signal characteristics and the sub-harmonic instability. Although the model presented in [6] and [7] is accurate and design oriented, it provides limited physical insight into the nature of current mode control because it consists of a combination of the *circuit* model of a power stage and a *block diagram* model of the current loop. Hence, neither the damping effect nor the sample-and-hold action of the current loop are easily discernible from the model.

In this paper, the concept of the PWM switch given in [8] and [9] is extended to develop an equivalent circuit model of current-mode control which yields essentially the same useful results given in [6] and [7]. In this case the original PWM switch and the current feedback are lumped together into a single three-terminal switching device, called the current-controlled, or current-programmed, PWM switch (CC-PWM), which is an invariant substructure of all current-mode controlled PWM converters. The parameters of the circuit model of the CC-PWM switch have very simple physical interpretations. For example, in the model of the CC-PWM switch operating in ccm and constant frequency the damping and sample-and-hold actions of the current feedback loop are modelled by a conductance, g_o, and a capacitance, C_s, respectively. The interaction of g_o and C_s with the rest of the converter can explain the observed small-signal behavior and the instability problem quite easily. For example, regardless of the particular topology, the model shows that the dynamics of the current loop

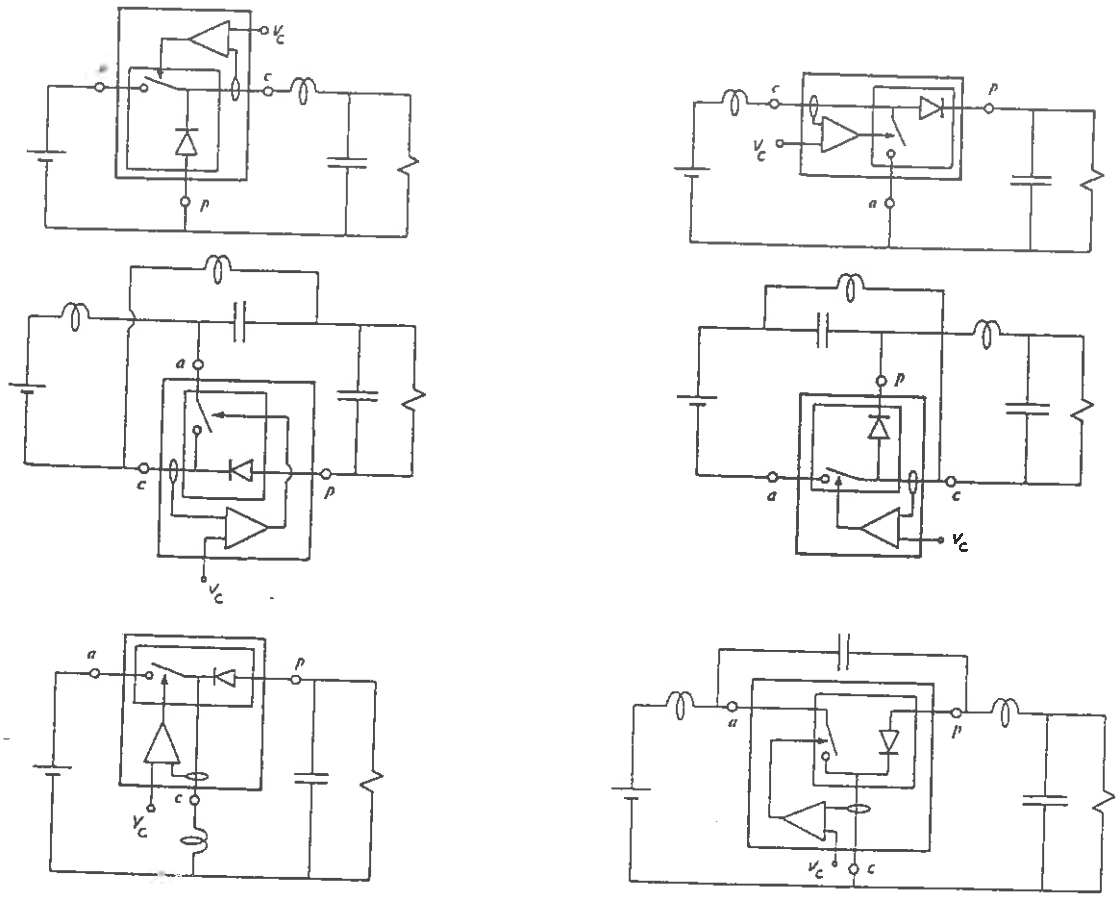

Fig. 1 The CC-PWM switch in six different converters

is given by a parallel resonance formed by C_s, g_o, and the filter inductor of the converter, L. This parallel resonant circuit is centered at half the switching frequency, $F_s/2$, because C_s is chosen to resonate with L at $F_s/2$. Hence, the small-signal characteristics exhibit a second-order resonance at $\omega_s/2$ damped by g_o. In the absence of an external ramp, g_o becomes negative for $D \geq 1/2$ causing the well-known sub-harmonic oscillation. Therefore, the equivalent circuit model of the CC-PWM switch provides good physical insight and is very easy to implement on circuit simulation programs such as Pspice.

An equivalent *circuit model* of the CC-PWM switch is derived in continuous conduction mode for the three known methods of current-mode control: constant frequency, constant off-time, and constant on-time. Several examples illustrating the use of the model are provided. Experimental results which verify the validity of the model are also presented.

MODEL OF THE CC-PWM SWITCH IN CONTINUOUS CONDUCTION MODE AND CONSTANT FREQUENCY OPERATION

Several PWM converters with only the current-loop closed are shown in Fig. 1. The major sub-structure that is common to all these converters is referred to as the *current-controlled PWM switch* and is shown in detail in Fig. 2. Since the terminals of the CC-PWM switch are the same as those of the PWM switch, it has the same *invariant* properties as the PWM switch [8] and [9]. Invariance is a consequence of the fact that the relationship between the *instantaneous* and *average* terminal voltages are the *same*, or invariant, regardless of the particular converter the switch is implemented in. The terminal voltages and currents of the PWM or CC-PWM switch operating in continuous conduction mode are shown in Fig. 3. The invariant relationship between the average terminal voltages and currents is easily seen to be:

$$\frac{i_a}{i_c} = \frac{v_{cp}}{v_{ap}} = d \qquad (1)$$

where $d = 1 - d'$ is the duty ratio. In current-mode control the slopes of the inductor, or the switch, current are important and their invariant relations (considering dc conditions for the moment) are given by:

$$S_n = \frac{V_{ac}}{L} R_i = \frac{V_{ap} D'}{L} R_i \qquad (2a)$$

$$S_f = \frac{V_{cp}}{L} R_i \qquad (2b)$$

where R_i is a scaling constant which transforms the current signal into a voltage signal. In order to see how Eqs. (2). apply to all the converters, consider the slope of the inductor current S_f/R_i given in Eq. (2b) during the off-time in the buck ($I_L = I_c$), boost ($I_L = -I_c$), buck-boost ($I_L = I_c$) and Cuk ($I_{L_1} + I_{L_2} = -I_c$) converters. These slopes can be determined from dc analysis and are given by:

$$\frac{S_f}{R_i} = \frac{\Delta I_c}{D' T_s} = \begin{cases} \dfrac{V_o}{L} & ; \text{ buck, buck-boost} \\ -\dfrac{V_o - V_g}{L} & ; \text{ boost} \\ -\dfrac{V_o}{L_1 \| L_2} & ; \text{ Cuk} \end{cases}$$

It can be easily see from the above that in each case when the input and/or output voltages are referred to the switch terminals, they are all equal to V_{cp} as given by Eq. (2b) (which is the meaning of invariance). A similar discussion applies to Eq. (2a).

The voltage and current waveforms for constant frequency operation with on-time control are shown in Fig. 4. The current waveform shown is the common terminal current, I_c, since it is the same as the switch current during the on-time. It can be easily seen from Fig. 4 that in the absence of any perturbations the following dc equation holds at the switching instant:

$$I_c R_i + \frac{S_f D' T_s}{2} + S_e D T_s = V_c \qquad (3)$$

In the remaining part of this section Eq. (3) will be perturbed, ignoring at first the sample-and-hold nature of the control, to obtain an average model of the switch which shows the damping effect of the current loop. Afterwards, the model will be augmented to incorporate the effect of the hold in the sample-and-hold action of the current loop.

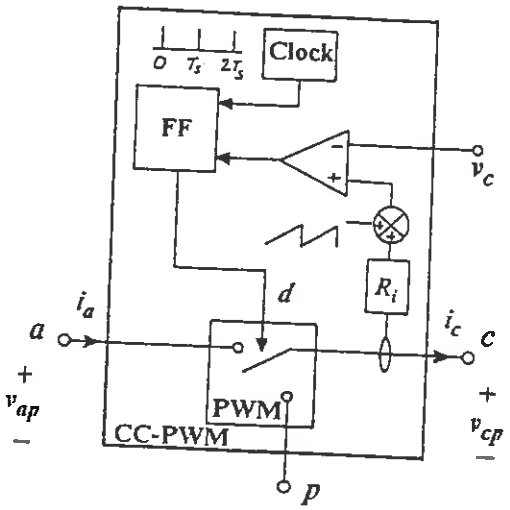

Fig. 2 The internal structure of the CC-PWM switch.

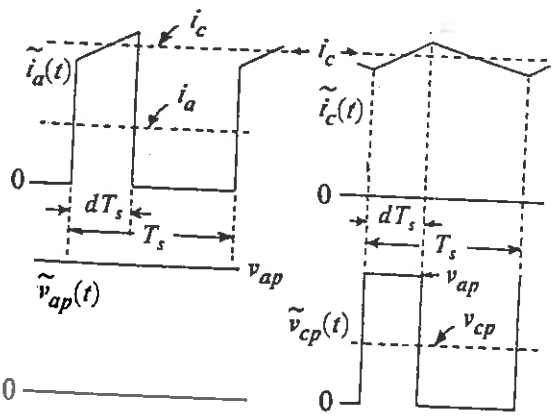

Fig. 3 The terminal voltages and currents of the CC-PWM switch.

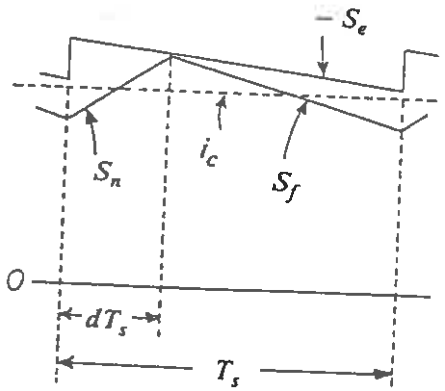

Fig. 4 The control action in constant frequency current-mode control.

A. Average model of the CC-PWM switch without the sample-and-hold effect.

Time *variations* in the *average* terminal current i_c, ignoring the sampling effect of the current loop, is given by Eq. (3) where the dc quantities are replaced by time-varying averages denoted by lower case letters:

$$i_c(t)R_i = v_c(t) - d(t)T_sS_e - \frac{s_f d'(t)T_s}{2} \qquad (4)$$

Whereas Eq. (3) is valid only at the switching instants DT_s, Eq. (4) is required to be valid for all time instants and as such is an average model. This equation is reexamined in the appendix. (It has been pointed out in [10] that when time variations are considered the control law is given by:

$$i_c(t)R_i = v_c(t) - d(t)T_sS_e - \frac{s_f d'^2(t)T_s}{2} - \frac{s_n d^2 T_s}{2}$$

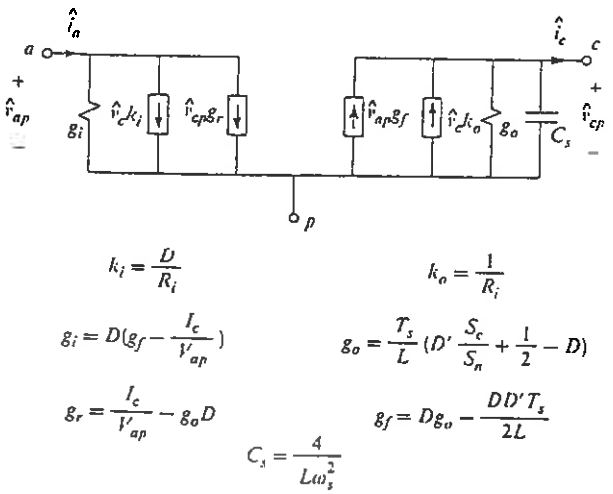

Fig. 5 The small-signal equivalent circuit of the CC-PWM switch.

instead of Eq. (4). Both equations, lead to the same small-signal model to be derived shortly as the reader can verify.) With this in mind, the duty-ratio and the slope s_f are substituted using Eqs. (1) and (2) in (4) to give:

$$i_c = \frac{v_c}{R_i} - \frac{v_{cp}}{v_{ap}} \frac{T_s S_e}{R_i} - v_{cp}\left(1 - \frac{v_{cp}}{v_{ap}}\right) \frac{T_s}{2L} \qquad (5a)$$

The average terminal current i_a is given by Eq. (1):

$$i_a = i_c \frac{v_{cp}}{v_{ap}} \qquad (5b)$$

Equations (5a) and (5b) are the invariant equations of the CC-PWM switch in constant frequency and ccm. Small-signal perturbations of Eqs. (5) gives:

$$\hat{i}_c = \hat{v}_c k_o + \hat{v}_{ap} g_f - g_o \hat{v}_{cp} \qquad (6a)$$

$$\hat{i}_a = \hat{v}_c k_i + \hat{v}_{cp} g_r + g_i \hat{v}_{ap} \qquad (6b)$$

where

$$k_o = \frac{1}{R_i} \qquad (7a)$$

$$k_i = Dk_o \qquad (7b)$$

$$g_o = \frac{T_s}{L}\left(D' \frac{S_e}{S_n} + \frac{1}{2} - D\right) \qquad (7c)$$

$$g_f = Dg_o - \frac{DD'T_s}{2L} \qquad (7d)$$

$$g_i = D\left(g_f - \frac{I_c}{V_{ap}}\right) \qquad (7e)$$

$$g_r = \frac{I_c}{V_{ap}} - g_o D \qquad (7f)$$

The small-signal equivalent circuit corresponding to these equations is shown in Fig. 5. Since the terminal voltages considered have the passive terminal in common, this model is referred to as the model of CC-PWM in the *common-passive* configuration. All the small-signal parameters are evaluated at the dc operating point denoted by capital letters. The switch capacitance C_s shown will be determined shortly.

The physical significance of the conductance g_o can be easily explained. The current feedback loop forces the average terminal current, i_c, to remain approximately at a constant value dictated by the reference signal which in turn causes port *cp* of the switch to look like current source with high incremental internal impedances. The effect of the external ramp, S_e, is to increase the value of this conductances reduce the damping, as can be seen from Eq. (7c). Hence, for very large values of the external ramp it can be seen that the CC-PWM looses its current-controlled properties and begins to behave like the PWM switch in continuous conduction mode. In fact, it can be easily shown that in the limit $S_e \to \infty$ the output circuit reduces to a voltage source $D\hat{v}_{ap}$ the input circuit reduces to a current source $D\hat{i}_c$:

$$\lim_{S_e \to \infty} \left[\frac{\hat{i}_a}{\hat{i}_c}\right] = \lim_{S_e \to \infty} \left[\frac{\hat{v}_{cp}}{\hat{v}_{ap}}\right] = D \qquad (8)$$

These results in the limit $S_e \to \infty$ reduce the model or CC-PWM to the simple model of the PWM switch in ccm without control as shown in Fig. 6. Hence, the transition from current-mode control to voltage-mode control as the external ramp is increased is shown to be a simple consequence of the increase in the switch conductance. In other words, the current-controlled PWM switch becomes a duty-ratio controlled PWM switch for large values of the external ramp.

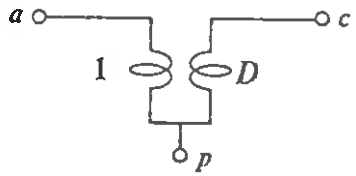

Fig. 6 Model of the PWM switch in ccm without control.

B. Modelling the effect of the sample-and-hold action.

Let the control and input voltages be held constant while the output voltage be replaced by a constant voltage source in any of the six PWM converters of Fig. 1. Figure 7a shows an example of the buck-boost converter under these conditions which are given by:

$$V_c = \text{const.} \Rightarrow \quad \hat{v}_c = 0 \tag{9a}$$

$$V_g, V_o = \text{const.} \Rightarrow \quad V_{ap} = \text{const.} \Rightarrow \quad \hat{v}_{ap} = 0 \tag{9b}$$

The small-signal equivalent circuit of *all* the PWM converters under the conditions of Eq. (9) is shown in Fig. 7b. In the following argument it will be shown that an arbitrary perturbation introduced in the converter will oscillate with a frequency $\omega_s/2$ which, according to the equivalent circuit in Fig. 7b, will set the value of C_s at $4/L\omega_s^2$. To do so, we refer to the steady-state waveforms shown in Fig. 8 where the inductor current is given an initial perturbation. (With the input, output and control voltages held constant, this can be done by shortening the off-time just for one cycle so that the inductor current will not return to its original value at the end of that cycle.) The inductor current will now evolve as shown by the broken line causing perturbations in the duty cycle at a frequency $\omega_s/2$ which in turn will cause the average port voltage v_{cp} to oscillate at the same frequency because we have:

$$v_{cp} = dV_{ap} \Rightarrow \quad \hat{v}_{cp} = \hat{d}V_{ap} \tag{10}$$

From this conclusion it follows that a perturbation in the inductor current in the equivalent circuit model in Fig. 7b should cause a perturbation in $\hat{v}_{cp}$

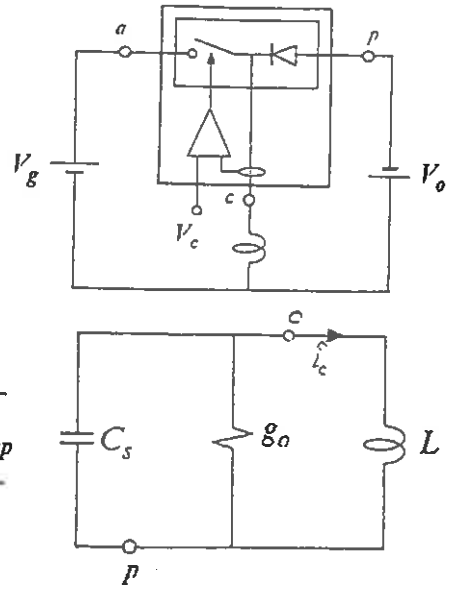

Fig. 7 a) the buck-boost converter b) the small-signal equivalent circuit.

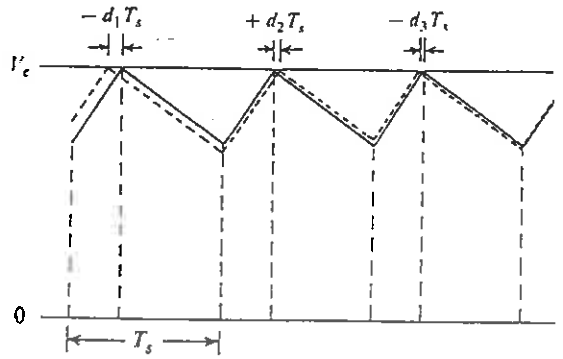

Fig. 8 The evolution of the current after an initial perturbation.

having a frequency $\omega_s/2$. Hence, from parallel resonance we have

$$\frac{\omega_s}{2} = \frac{1}{\sqrt{LC_s}} \Rightarrow \quad C_s = \frac{4}{L\omega_s^2} \tag{11}$$

This completes the equivalent circuit model of the CC-PWM in CCM constant frequency operation with on-time control. Further comments and conclusions are given in the appendix.

A physical interpretation of the switch capacitance, C_s, is that it models the the holding action of the current loop in *ccm*. After all, a capacitor is the simplest circuit element that can hold a voltage across it for a characteristic period of time. This observation leads to the conclusion that in dcm this capacitance should disappear because the holding action of the current loop is no longer present.

C. The stability problem and the significance of g_o.

The stability of the current loop can be easily studied from the parallel resonant circuit shown in Fig. 7b which was obtained under the conditions given in Eqs. (9). This circuit approximates very closely the dynamic behavior of the current loop for *all* PWM converters near the vicinity of half the switching frequency because the output filter capacitor essentially acts like a short circuit at these frequencies. With the inputs held fixed and the output ac-shorted, the conditions in Eqs. (9) are satisfied. It can now be seen from Fig. 7b that the only damping element is the conductance g_o which, in the absence of an external ramp, is given by:

$$g_o = \frac{T_s}{L}\left(\frac{1}{2} - D\right) \quad ; \quad S_e = 0 \tag{12}$$

If $D \geq 1/2$, then g_o is negative and the current loop oscillates. This oscillation is a sub-harmonic oscillation because the frequency of the unstable pole-pair is at half the switching frequency, $\omega_s/2$. If an external ramp is added, the conductance can remain positive for higher values of D. This example explains the stability problem using physical models only.

Finally, we note that the parallel resonant circuit in Fig. 7b, representing the dynamics of the current loop, will contribute a complex pair of poles given by:

$$\Delta(s) = 1 + sLg_o + \frac{s^2}{(\omega_s/2)^2} \tag{13a}$$

Upon substitution for g_o in the above gives:

$$\Delta(s) = 1 + \frac{s}{Q\omega_s/2} + \frac{s^2}{(\omega_s/2)^2} \tag{13b}$$

where

$$Q = \frac{1}{\pi(D'\frac{S_e}{S_n} + \frac{1}{2} - D)} \tag{13c}$$

Since the switch model is independent of a particular topology, this pole-pair, to an excellent approximation, appears in *all* the small-signal transfer functions of constant frequency, current-mode controlled converters operating in ccm. In other words, when the transfer functions of these converters are determined, $\Delta(s)$ in Eq. (13) will be an approximate factor of the denominator because the damping due to the load will be insignificant at $\omega_s/2$. An example illustrating this point will be worked out later for the buck-boost converter. As discussed in [6], this quadratic causes a peaking in the transfer functions at $\omega_s/2$ whose Q depends on the duty ratio and the external ramp as given by Eq. (13c).

CONSTANT OFF-TIME AND CONSTANT ON-TIME MODELS OF THE CC-PWM SWITCH IN CCM

The need for an external ramp to stabilize current-mode controlled converters can be eliminated if variable frequency operation is allowed. The two known methods are the constant on-time and constant off-time methods. The models corresponding to these two schemes are derived below.

A. Constant off-time control.

In this method of control, turn-on is initiated after a fixed turn-off time and the active switch conducts for a variable period of time until the current reaches a fixed threshold level. The waveforms corresponding to this method of control are shown in Fig. 9 whence we have under dc conditions:

$$I_c = \frac{V_c}{R_i} - V_{cp}\frac{T_{off}}{2L} \tag{14}$$

When time variations are considered, the control law in Eq. (14) has the following form:

$$i_c(t) + \frac{di_c(t)}{dt}\frac{t_{on}}{2} = \frac{1}{R_i}v_c(t + \frac{t_{on}}{2}) - v_{cp}(t)\frac{T_{off}}{2L} \tag{15}$$

Admittedly, Eq. (15) is not obvious save for the fact that under dc conditions it reduces to Eq. (14). Two explanations will be given for the presence of the first-order derivative in Eq. (15). The first explanation is based on graphical construction of the waveforms under a perturbation in the control voltage keeping the slopes constant as shown in Fig. 10. Here, the on-time is purposely shown to be much longer than the off-time because the derivative in Eq. (15) becomes important only when $T_{on} >> T_{off}$ and the explanation becomes more obvious. Thus it becomes necessary to reexamine the expressions of the slopes which under a transient condition are given by:

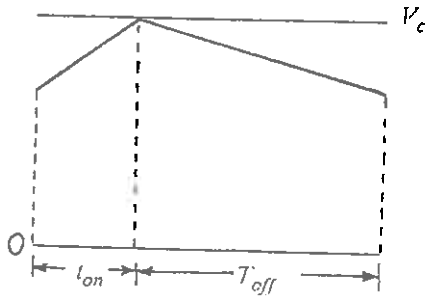

Fig. 9 The control action in constant off-time control.

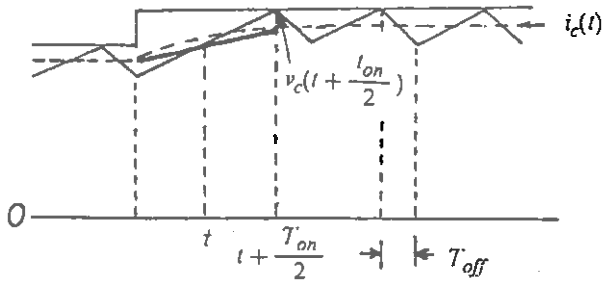

Fig. 10 The evolution of the current in response to a perturbation in v_c

$$\frac{s_n}{R_i} = \frac{v_{ac}}{L} + \frac{di_c}{dt} \tag{16a}$$

$$\frac{s_f}{R_i} = \frac{v_{cp}}{L} - \frac{di_c}{dt} \tag{16b}$$

These expressions are obtained by accounting for the the inductor voltage Ldi_c/dt during a transient as can be verified from any one of the converters. An *average* control law (as opposed to sampled-data) which is written in reference to the average current $i_c(t)$ and the slope s_n, can only *approximately* account for $i_c(t)$ and its evolution $di_c(t)/dt$. The simplest approximation which describes the evolution of $i_c(t)$ is a straight-line approximation. This approximation will be used in deriving the control laws for constant off-time and constant on-time. (The control law for constant frequency is reexamined in the appendix.)

It can be seen from Fig. 10 that the *average* current, $i_c(t)$, has increased and that this increase has taken place mostly during t_{on}. The exact evolution of $i_c(t)$, shown in dotted lines, is not known *apriori* but with a straight line approximation, shown in solid lines, the control law can be written as follows:

$$i_c(t) + s_n \frac{t_{on}}{2} = \frac{1}{R_i} v_c(t + \frac{t_{on}}{2}) \tag{17}$$

where s_n is given by Eq. (16a) in which the derivative, di_c/dt, is the slope of the straight approximation of the evolution of $i_c(t)$. Substituting for s_n in the above, we get:

$$\frac{1}{R_i} v_c(t + \frac{t_{on}}{2}) = \tilde{i}_c(t) + \left[\frac{v_{ac}(t)}{L} + \frac{di_c(t)}{dt} \right] \frac{t_{on}}{2} \tag{18}$$

Equation (15) follows by substituting for v_{ac} which can be obtained from Eq. (1) as follows:

$$\frac{v_{cp}}{v_{ap}} = \frac{t_{on}}{t_{on} + T_{off}} \Rightarrow v_{ac} = v_{cp} \frac{T_{off}}{t_{on}} \tag{19}$$

In light of the above, a reexamination of the control law for constant frequency given in Eq. (4) is presented in the appendix.

Equation (15) is perturbed by letting $i_c = I_c + \hat{i}_c$ and $t_{on} = T_{on} + \hat{t}_{on}$ and ignoring second order terms. This yields:

Equation (15) is perturbed by letting $i_c = I_c + \hat{i}_c$ and $t_{on} = T_{on} + \hat{t}_{on}$ and ignoring second order terms. This yields:

$$\hat{i}_c(t) + \frac{d\hat{i}_c(t)}{dt} \frac{T_{on}}{2} = \frac{1}{R_i} \hat{v}_c(t + \frac{T_{on}}{2}) - \hat{v}_{cp}(t) \frac{D'T_s}{2L} \tag{20}$$

The Laplace transform of Eq. (20) yields:

$$\hat{i}_c = \hat{v}_c k_o - g_o \hat{v}_{cp} - \hat{i}_c s\tau_o \tag{21}$$

where

$$\tau_o = \frac{DT_s}{2} \tag{22a}$$

$$k_o = \frac{e^{s\tau_o}}{R_i} \tag{22b}$$

$$g_f = 0 \tag{22c}$$

$$g_o = \frac{D'T_s}{2L} \tag{22d}$$

The parameters of the input circuit are obtained, as before, from a perturbation of Eq. (5b):

$$\hat{i}_a = \hat{v}_c k_i + v_{cp} g_r + g_i \hat{v}_{ap} - \hat{i}_c s\tau_i \tag{23}$$

where

$$\tau_i = \tau_o D \tag{24}$$

The remaining parameters are given in Eqs. (7b,e,f). The general model, which includes an external ramp, is given in Fig. 15.

The contribution of the current loop to the dynamics of all current-mode controlled converters with constant off-time (and no external ramp, i.e., $S_e = 0$) can now be determined from the circuit in Fig. 11 which is obtained under the conditions given in Eqs. (9a,b). The poles due to the current loop are thus given by:

$$\Delta(s) = 1 + s(Lg_o + \tau_o) + s^2 LC_s \tag{25a}$$

Substitution of Eqs. (22a) and (22d) yields:

$$\Delta(s) = 1 + \frac{s}{Q\omega_s/2} + \frac{s^2}{(\omega_s/2)^2} \tag{25b}$$

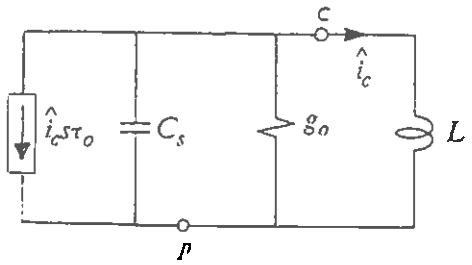

Fig. 11 The small-signal circuit for the determination of the dynamics of the current loop in constant off-time control

where

$$Q = \frac{2}{\pi} \tag{25c}$$

The Q of this quadratic is fixed and independent of the operating point as has been pointed out in [7]. The fact that the damping should be independent of the operating point can be graphically explained as shown in Fig. 12 where a perturbation in the inductor current is considered for two different operating points. First, it can be seen that the response is non-oscillatory and second, regardless of the operating point, the circuit always recovers in exactly one switching period. These two observations provide the second explanation for the presence of the derivative in Eq. (15). The frequency dependent current source, which properly adjusts the high-frequency damping (without effecting the dc damping), is the Laplace transform of the derivative $d\hat{i}_c/dt$. Without this adjustment, the Q would have been $Lg_o = 2/\pi D'$ which for small values of D', or $T_{on} >> T_{off}$, would have predicted, incorrectly, an oscillatory response.

B. Constant on-time control.

In this method of control turn-off is initiated after a fixed period of on-time. The off-time is terminated when the falling current ripple reaches a threshold level set by the control voltage. The current waveforms for this method of control are shown in Fig. 13 whence it is clear that:

$$i_c R_i = v_c(t + \frac{t_{off}}{2}) + \frac{s_f t_{off}}{2} \tag{26}$$

Substitution of Eq. (16b) in the above followed by a perturbation gives:

$$\hat{i}_c = \frac{1}{R_i}\hat{v}_c(t + \frac{T_{off}}{2}) + \hat{v}_{cp}\frac{D'T_s}{2L} + \frac{V_{cp}}{2L}\hat{t}_{off} - \frac{d\hat{i}_c}{dt}\frac{T_{off}}{2} \tag{27}$$

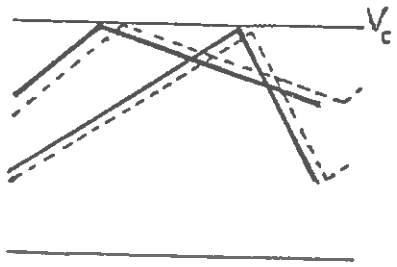

Fig. 12 The response of constant off-time at two different operating points.

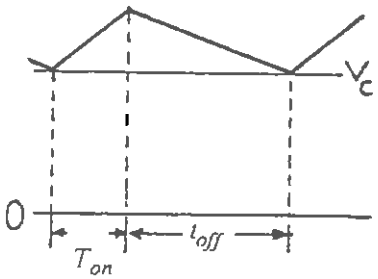

Fig. 13 the control action in constant on-time control.

Since the frequency is being modulated along with the duty-ratio, the perturbation in t_{off} is obtained by perturbing the following equation:

$$\frac{T_{on}}{T_{on} + t_{off}} = \frac{v_{cp}}{v_{ap}} \tag{28}$$

which gives

$$-\frac{T_{on}}{T_s^2}\hat{t}_{off} = \frac{\hat{v}_{cp}}{V_{ap}} - \frac{V_{cp}}{V_{ap}^2}\hat{v}_{ap} \tag{29}$$

Substitution of Eq. (29) in (27) gives:

$$\hat{i}_c = \frac{1}{R_i}\hat{v}_c(t + \frac{T_{off}}{2}) + \hat{v}_{ap}\frac{DT_s}{2L} - \hat{v}_{cp}\frac{DT_s}{2L} - \frac{d\hat{i}_c}{dt}T_{off} \tag{30}$$

The Laplace transform of the above is:

$$\hat{i}_c = \hat{v}_c k_o + g_f\hat{v}_{ap} - g_o\hat{v}_{cp} - \hat{i}_c s\tau_o \tag{31}$$

where:

$$\tau_o = \frac{D'T_s}{2} \tag{32a}$$

$$g_f = g_c = \frac{DT_s}{2L} \tag{32b}$$

$$k_o = \frac{e^{s\tau_o}}{R_i} \tag{32c}$$

The small-signal parameters of the input circuit are obtained the same way as in Eqs. (21) and (22). The general model, which includes an external ramp, is shown in Fig. 15.

The contribution of the current-loop to the dynamics of constant on-time converters is exactly the same as that of constant off-time converters given in Eq. (25b). This is expected because the damping should be independent of the operating point for the same reasons given for constant off-time control.

C. A simple example.

From the expression of $\Delta(s)$, given in Eq. (25b), for constant on-time and constant off-time control, it can be seen that these controllers will never suffer from any *sub-harmonic* instability and no stabilizing ramp is necessary. This does not mean that converters which employ these types of control will not oscillate at all. This point and another interesting feature of constant off-time control are illustrated in the following example.

A buck converter with an input filter and constant-off time control is shown in Fig. 14a. From the equivalent circuit model in Fig. 14b, it can be seen that the line-to-output transfer function is zero for all operating conditions because $g_f = 0$ as given Eq. (20c). This circuit, however, will suffer from input filter oscillations at all operating conditions because the switch conductance, given by Eq. (7c), is negative:

$$g_i = -\frac{DI_c}{V_{ap}} = -\frac{DI_o}{V_g} = -\frac{DM}{R} = -\frac{D^2}{R} \quad (33)$$

As pointed out earlier, the source of this instability is not the current loop, but the input filter. This instability can be removed by proper input filter design as discussed in [11].

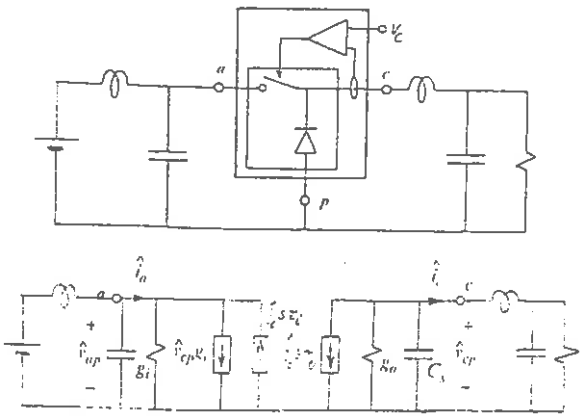

Fig. 14 a) Buck converter b) equivalent circuit for constant off-time.

GENERAL MODEL OF THE CC-PWM SWITCH IN CCM

The results obtained in the previous section can be summarized in a single model, shown in Fig. 15, for all three cases where the output parameters are given by:

$$g_o = \frac{T_s}{L}\left[\alpha\frac{S_e}{S_n} + \beta\frac{D'}{2} - \gamma D\left(\frac{S_e}{S_n} + \frac{1}{2}\right)\right] \quad (34)$$

$$g_f = D\left(g_o - \beta\frac{D'T_s}{2L}\right) \quad (35)$$

$$\tau_o = \frac{DT_s}{2}(\beta - \gamma) \quad (36)$$

$$k_o = \frac{e^{s\tau_o}}{R_i} \quad (37)$$

where

$$\alpha = \beta = \gamma = 1 \quad \text{const.} F_s \quad (38a)$$

$$\alpha = \beta = 1,\ \gamma = 0 \quad \text{const. } T_{off} \quad (38b)$$

$$\alpha = \frac{D'}{D} - 1,\ \beta = -1,\ \gamma = \frac{-1}{D} \quad \text{const. } T_{on} \quad (38c)$$

These results are general and include the case of an external ramp in constant on-time and constant off-time control. The remaining input parameters are given by Eqs. (7b,e,f) and (24).

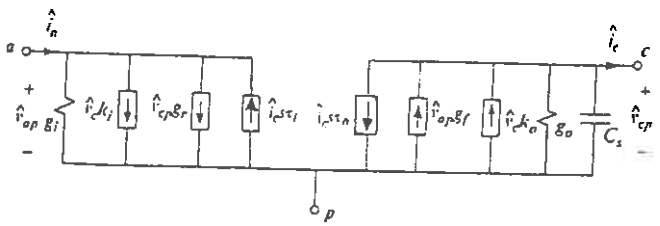

Fig. 15 General equivalent circuit for current mode control. The parameters are given in the text.

ANALYSIS OF CURRENT-MODE CONTROLLED CONVERTERS

In this section the model of the CC-PWM switch is used to analyze the buck-boost and boost converters. In each case, the CC-PWM switch is replaced by its equivalent circuit model in which the small-signal parameters are evaluated at the dc operating point. The various transfer functions are then obtained by simple network analysis.

A. The buck-boost converter in ccm with constant frequency current-mode control.

This converter is shown in Fig. 16. The small-signal characteristics are determined by substituting the small-signal model of the CC-PWM as outlined in the previous section.

The line-to-output transfer function.

For the determination of this transfer function V_g is replaced by a signal source $\hat{v}_g$ and the CC-PWM is replaced by its equivalent circuit model of Fig. 5 as shown in Fig. 17. The control sources are removed because of open-loop considerations. The transfer function is of the form:

$$\frac{\hat{v}_o}{\hat{v}_g} = A_l \frac{N(s)}{D(s)} \tag{39}$$

Each component of Eq. (39) can be determined independently by a special manipulation of the circuit in Fig. 17. For the determination of A_l we need consider the circuit under dc condition which gives:

$$A_l = \frac{g_l - g_f}{\Sigma g} = M \frac{\frac{K_c}{K}(M - 2\frac{S_e}{S_n}) - M}{\frac{K_c}{K}(1 + 2\frac{S_e}{S_n}) + 2M + 1} \tag{40}$$

where

$$K_c = D'^2 \quad ; \quad K = \frac{2LF_s}{R} \tag{41}$$

The denominator is of third-order and is determined by the use of the method of time constants:

$$D(s) = 1 + a_1 s + a_2 s^2 + a_3 s^3 \tag{42}$$

where

$$a_1 = L\frac{g_o(g_i + G) + g_f g_r}{g_i + G - g_f} + \frac{C_s + C}{\Sigma g} \tag{43a}$$

$$a_2 = \frac{LCg_o}{\Sigma g} + C_s L \frac{(g_i + G)}{\Sigma g} \tag{43b}$$

$$a_3 = \frac{CC_s L}{\Sigma g} \tag{43c}$$

$$\Sigma g = g_o + g_i - g_f + g_r + G \tag{43d}$$

It may be shown, either numerically or analytically, that a_1 and a_2 can be approximated as follows:

$$a_1 = \frac{C}{\Sigma g} \quad ; \quad a_2 = \frac{LCg_o}{\Sigma g} \tag{44}$$

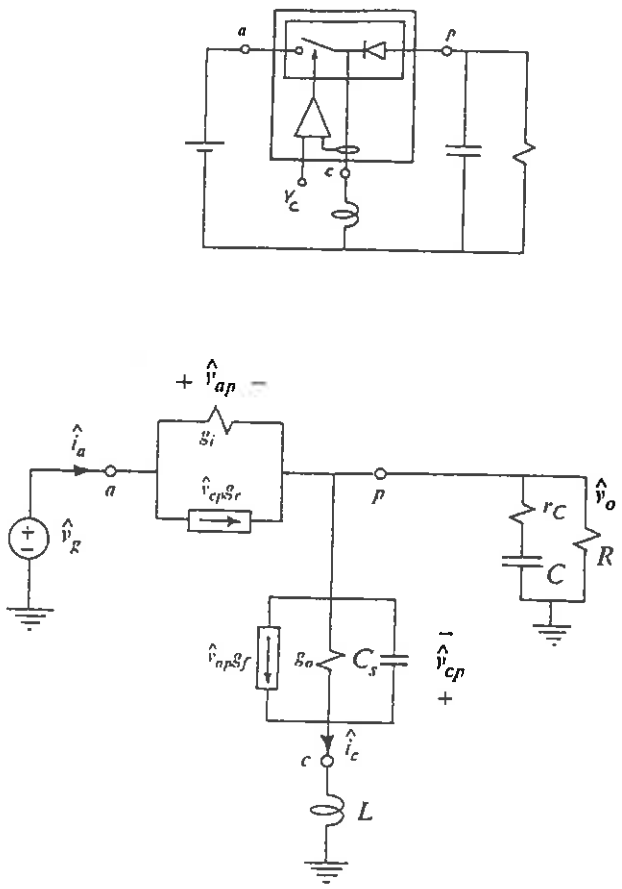

Fig. 16 a) The buck-boost converter b) equivalent circuit for the line-to-output transfer function.

This leads to the approximate factorization of the denominator as follows:

$$D(s) = (1 + s\frac{C}{\Sigma g})(1 + sLg_o + s^2 LC_s) \tag{45}$$

The quadratic factor is seen to be the same as the one in Eq. (13) which is the contribution of the current loop. The expression of the dominant pole is obtained by the use of Eqs. (7)

$$s_{p1} = \frac{\Sigma g}{C} = \frac{D'\frac{K_c}{K}(1 + 2\frac{S_e}{S_n}) + 1 + D}{RC} \tag{46}$$

Deep into continuous conduction mode $K >> K_c$ this pole is approximately given by:

$$s_{p1} \simeq \frac{(1 + D)}{RC} \quad ; \quad K >> K_c \tag{47}$$

The only zero in the numerator is the one given by the esr of the output filter capacitor. This will be seen to be true when the zeroes of the control-to-output transfer function are determined. Hence, the line-to-output transfer function is given by:

$$\frac{\hat{v}_o}{\hat{v}_g} = A_l \frac{1 + s/s_{z1}}{(1 + \frac{s}{s_{p1}})(1 + \frac{s}{Q\omega_s/2} + \frac{s^2}{(\omega_s/2)^2})} \quad (48)$$

where $s_{z1} = 1/r_c C$ and Q is the same as in Eq. (13c).

The control-to-output transfer function.

Since the denominator of this transfer function is the same as the one given in Eq. (48), only the low-frequency asymptote and the numerator need to be determined. From Fig. 18, the low frequency asymtote is given by:

$$A_c = \frac{k_i - k_o}{\Sigma g} = -\frac{R}{R_i} \frac{1}{\frac{K_c}{K}(1 + 2\frac{S_e}{S_n}) + 2M + 1} \quad (49)$$

The zeroes of the transfer function are obtained by studying the circuit under null conditions of the output in the transform domain. The first null is given by the zero of the impedance $r_c + 1/sC$ which is the zero of the output filter capacitor. The second null is given by the null in the terminal current $i_p(s_z) = 0$ as shown in Fig. 18. From the null conditions shown in Fig. 18 two equations are obtained. The first is given by $i_a(s_z) = i_c(s_z)$ which gives

$$g_r \hat{v}_{cp} + k_i \hat{v}_c = \frac{\hat{v}_{cp}}{s_z L} \quad (50a)$$

The second equation is obtained from the condition that the sum of the currents in g_o, C_s and $k_o \hat{v}_c$ must equal to the current in L:

$$-\hat{v}_{cp}(g_o + s_z C_s) + k_o \hat{v}_c = \frac{\hat{v}_{cp}}{s_z L} \quad (51b)$$

The simultaneous solution of Eqs. (50a) and (50b) gives:

$$N(s_z) = s_z^2 \frac{LC_s k_i}{k_i - k_o} + s_z L \frac{k_i g_o + k_o g_i}{k_i - k_o} + 1 = 0 \quad (52a)$$

Substitution of the expressions for the small-signal parameters from Eqs. (7) yields the numerator $N(s)$:

$$N(s) = s^2 LC_s \frac{D}{D'} - s\frac{LD}{D'^2 R} + 1 \quad (52b)$$

The roots of this equation are well separated and can be approximately factored as follows:

$$N(s) = (1 - s\frac{DL}{D'^2 R})(1 + sRC_s D') \quad (52c)$$

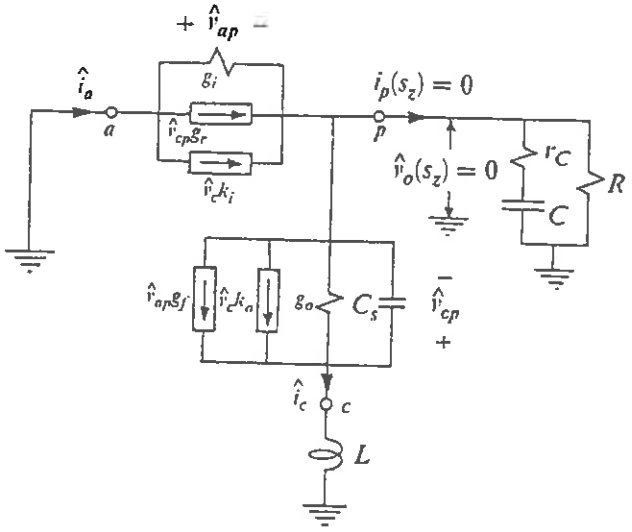

Fig. 17 Equivalent circuit of the buck-boost for control-to-output transfer function.

Hence the control-to-output transfer is given by:

$$\frac{\hat{v}_o}{\hat{v}_c} = A_c \frac{(1 + \frac{s}{s_{z1}})(1 - \frac{s}{s_{z2}})(1 + \frac{s}{s_{z3}})}{(1 + \frac{s}{s_{p1}})(1 + \frac{s}{\omega_n Q} + \frac{s^2}{\omega_n^2})} \quad (72)$$

where

$$s_{z2} = \frac{D'^2 R}{DL} \quad (54a)$$

$$s_{z3} = \frac{1}{RC_s D'} = \frac{\pi^2 K}{\sqrt{K_c}} \frac{F_s}{2} >> \frac{F_s}{2} \quad (54b)$$

The second zero is the usual r.h.p. zero of the buck-boost converter in ccm. The third zero is considerably far out that it can be ignored. The presence of this third zero in the transfer function presents a minor discrepancy between the model of CC-PWM and the model in [6].

B. The boost converter in ccm.

The example of the boost converter discussed in [2] is used here to illustrate the simplicity of the model of the CC-PWM switch and its accuracy. The circuit parameters in that example are given by:

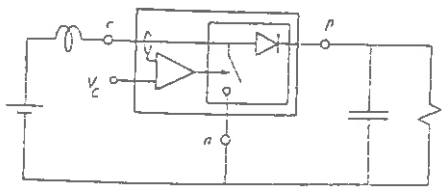

$$L = 390\mu H \quad C = 24\mu F \quad R = 75\Omega$$

$$D = .55 \quad V_o = 25V \quad F_s = 25kHz \quad S_e = S_f$$

The elements of the switch model are then computed from Eqs. (7) as follows:

$$g_o = 1.832 \times 10^{-2} \quad g_f = 5.542 \times 10^{-3} \quad \Omega^{-1}$$

$$g_r = 1.956 \times 10^{-2} \quad g_i = -2.4 \times 10^{-2} \quad \Omega^{-1}$$

$$R_i = 1.5\Omega \quad k_o = .6666 \quad k_i = .3666$$

$$C_s = 4.619 \times 10^{-8} \mu F$$

The following Pspice program was written to determine the various transfer functions. The control-to-output transfer function is shown in Fig. 19. The agreement with the experimental results is very good. The predictions given in Ref. [2], using extended state-space averaging (ESSA), are also shown in dashed lines.

```
Vg 10 0 ac 1
Vc 7 8 ac 0
L1 1 2 390uH
Rsense 10 1 1e-6
R  3 0 75
C  3 0 24uF
X1 0 3 2 7 8 CP-PWMSM1
.ac dec 80 10Hz 100Khz
.probe
.print ac idb(Rsense) ip(Rsense)
.subckt CP-PWMSM1 1 2 3 4 5
ri 1 2 -75.5
Gki 1 2 4 5 .3666
Gr 1 2 3 2 1.956E-2
Gf 2 3 1 2 5.542e-3
Gko 2 3 4 5 .6666
ro 3 2 54.6
cs 3 2 4.619E-8
r1 4 5 1G
r2 5 2 1G
.ends
.end
```


Aknowledgment

I would like to thank my colleague Ray Ridley with whom I have had many hours of discussion on current mode control and whose work ([6] and [7]) for the first time kindled my interest in the analysis of current mode control. The purpose of this work, as stated in the introduction, was to develop a self-contained circuit model which yields the same results with some minor differences.

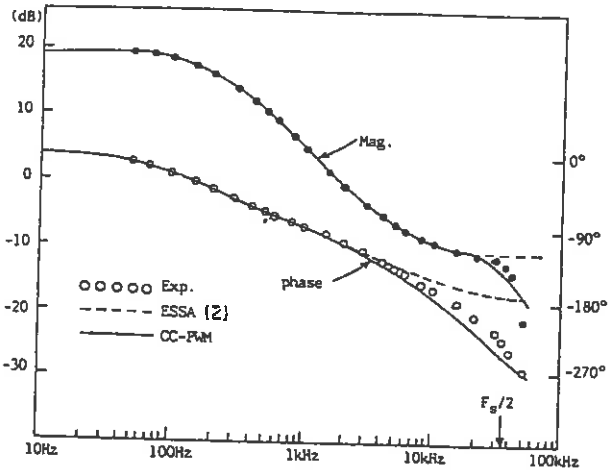

Fig. 18 Experimental and predicted results of the boost converter.

APPENDIX

In this appendix the control law for constant frequency given by Eq. (4) is reexamined in light of Eqs. (16). The evolution of the *instantaneous* current (triangular shape), $\tilde{i}_c(t)$, under a perturbation is repeated here in Fig. A.1. It can be seen that the evolution of the average current, $i_c(t)$, must be sinusoidal (of yet unknown damping and amplitude) as shown in Fig. A.2 in dashed lines. The best straight line approximation of $i_c(t)$ with respect to which the control law can be written is shown in solid lines. Hence, in writing the control law, the $di_c(t)/dt$ term, in the expression of s_f must be zero as considered in Eqs. (4) and (5a).

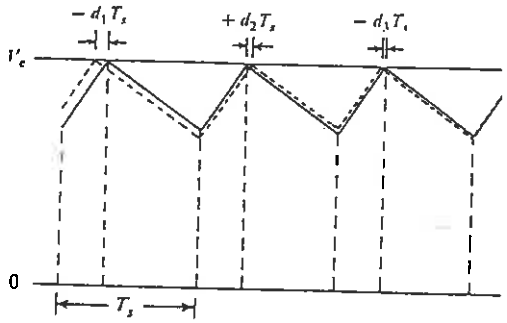

Fig. A.1

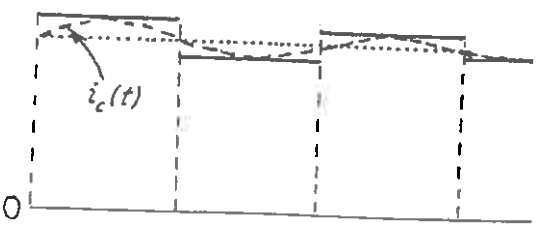

Fig. A.2

It should be pointed, as a final remark, that the oscillatory behavior of $\hat{v}_{cp}$ predicted in Fig. 7b (which led to the determination of C_s in Eq. (11)) is *not* in contradiction with the fact that the slopes of the current where held constant in arriving at that conclusion. The reason is that the slopes under a transient condition are always given by Eq. (16) which, according to Fig. 7b, remain unchanged because $\hat{s}_f = \hat{v}_{cp}/L - \hat{di_c}/dt = 0$.

REFERENCES

[1] Cecil W. Deisch, "Switching Control Method Changes Power Converter into a Current Source," IEEE Power Electronics Specialist Conference, 1978 Record, pp. 300-306, (IEEE Publication 78CH1337-5 AES).

[2] S. Hsu, A. Brown, L. Rensink and R.D. Middlebrook, "Modelling and Analysis of Switching Dc-to-Dc Converters in Constant Frequency Current-Programmed Mode," IEEE Power Electronics Specialist Conference, 1979 Record, pp. 284-301, (IEEE Publication 79CH1461-3 AES).

[3] R.D. Middlebrook, "Topics in Multi-Loop regulators and Current-Mode Programming," IEEE Power Electronics Specialist Conference, 1985 Record, pp. 716-732, (IEEE Publication 85CH2117-0).

[4] A.S. Kislovski, "Introduction to Dynamical Analysis of Switching dc-dc Converters," (a monograph), EMV Engineering, Loechliweg 47, 3000 Berne, Switzerland, 1985.

[5] Art Brown and R.D. Middlebrook, "Sampled-Data Modelling of Switching Regulators," IEEE Power Electronics Specialist Conference, 1981 Record, pp. 349-369. (IEEE Publication 81CH1652-7).

[6] R. Ridley, "A New, Continuous-Time Model For Current-Mode Control," Power Conversion and Intelligent Motion Conference, Oct. 16-19, 1989.

[7] R. Ridley, "A New, Continuous-Time Model For Current-Mode Control with Constant Frequency, Constant On-Time, and Constant Off-Time in CCM and DCM," IEEE Power Electronics Specialist Conference, 1990 Record, pp. 382-389. (IEEE Publication 90CH2873-8).

[8] V. Vorpérian, "Simplified Analysis of PWM Converters Using the Model of The PWM Switch, Part I: Continuous Conduction Mode", AES May 1990 Vol. 26, No. 3, pp. 490-496.

[9] V. Vorpérian, "Simplified Analysis of PWM Converters Using the Model of The PWM Switch, Part II: Discontinuous Conduction Mode", AES May 1990 vol. 26, No. 3, pp. 496-505.

[10] G.C. Verghese, C.A. Bruzos, K.N. Mahabir, "Averaged and Sampled-Data for Current-Mode Control," IEEE Power Electronics Specialist Conference, 1989 Record, pp. 484-491. (IEEE Publication 89CH2721-9)

[11] R.D. Middlebrook, "Design Techniques For Preventing Input-Filter Oscillations in Switched Mode Regulators," Proceedings of the Fifth National Solid-State Power Conversion Conference, Powercon 5, 1978, pp. A3.1 - A3.16.